Resistive switching characteristics and mechanism of thermally grown WO_x thin films

Kuyyadi P. Biju,[1,2,a)] Xinjun Liu,[3] Manzar Siddik,[1] Seonghyun Kim,[3] Jungho Shin,[1] Insung Kim,[3] Alex Ignatiev,[1,b)] and Hyunsang Hwang[1,3,c)]
[1]*Department of Nanobio Materials and Electronics, Gwangju Institute of Science and Technology, Gwangju 500-712, South Korea*
[2]*Department of Physics, Government College Kodenchery, Calicut 673580, India*
[3]*School of Materials Science and Engineering, Gwangju Institute of Science and Technology, Gwangju 500-712, South Korea*

(Received 4 February 2011; accepted 3 August 2011; published online 19 September 2011)

Resistive switching characteristics of thermally oxidized tungsten thin films and their switching mechanism were investigated, modifying thickness of the active layer (WO_x) by varying oxidation conditions. Two types of switching were observed in $Pt/WO_x/W$ memory devices. Thinner film ($t \leq 15$ nm) exhibits clockwise switching (CWS) with filamentary characteristics, whereas thicker film ($t \geq 25$ nm) exhibits counter-clockwise switching (CCWS) with more homogeneous conduction. Both switching modes are highly reliable and show good cycling endurance. The conduction phenomena in two different switching modes were examined. In the case of CWS, the conduction mechanism changes from Schottky emission to ohmic conduction due to the local bypass of Schottky barrier formed at Pt/WO_x interface by oxygen vacancies. Contrary to CWS, CCWS showed a completely different conduction mechanism. The high resistance state is dominated by the Schottky emission at low electric field and by Poole–Frenkel emission at high electric field, whereas the low resistance state exhibits the Schottky emission. Different types of switching behavior might be attributed to the non-homogenous defect distribution across the active layer. A possible conduction sketch for two types switching behaviors is also discussed. © *2011 American Institute of Physics*. [doi:10.1063/1.3633227]

I. INTRODUCTION

Electric-field-induced resistive switching (RS) in binary and complex oxides has aroused great interest because of its potential application in the next generation of nonvolatile memory devices.[1–3] RS behavior is classified as unipolar or bipolar, depending on the programming and erasing polarity of the applied voltage.[1,4] In unipolar switching, the resistance change takes place irrespective of the pulse polarity, while the bipolar switching requires the polarity to be reversed. The coexistence of both switching behaviors in a single material such as NiO,[5] TiO_2,[6] $BaSrTiO_3$,[7] and ZnO (Ref. 8) have received considerable attention in recent times. On the basis of the switching mechanism, RS can be classified into filamentary-type and interface-type (or homogeneous) switching.[1,4] The distribution of switching currents is highly localized in typical filamentary switching while it is homogeneously distributed across the device area in interface type. Coexistence of filamentary and homogeneous RS in Sr_2TiO_4 and Fe-doped $SrTiO_3$ thin films were reported recently.[9,10] Even though the driving mechanism of resistive switching phenomena has not been completely established, there exists a general agreement that the migration of oxygen ions or vacancies under an applied electric field plays a key role in resistive switching. However, there have been several concerns regarding the switching location where the resistance change mainly occurs. In the case of unipolar resistive switching, switching location was reported to be localized at the anode, cathode, or the middle, while bipolar resistive switching localized at the electrode interface with Schottky barrier modification or local modification of broken filaments by oxygen vacancy movement.[2,7,11–14] Even with all these differences, each case may follow the same fundamental mechanism of electron-ion dynamics. In most studies, oxygen interaction between a metal oxide and metal electrode has been reported as the dominant mechanism for switching behavior. By selecting different electrodes, Peng *et al*. have shown both interface and filamentary-type switching in Mn-doped ZnO.[15] Here we observed two different types of resistive switching in WO_x film with Pt as the top electrode.

Tungsten oxide is a widely studied material for the development of solid-state device application such as electrochromics and gas sensors. Tungsten is a widely accepted material in the microelectronics industry, especially in multilevel interconnects. Further, tungsten offers a high degree of compatibility and ease of processing within the overall structure of the integrated circuit when WO_3 is used as active material in resistance random access memory (RRAM).[16–19] Here we opted for thermal oxidation process to prepare tungsten oxide layers because it allows, in comparison to thin film deposition techniques, easy self-aligned process integration. The switching phenomena in these material systems are controversially explained as filament formation or interfacial barrier potential induced by electron trapping and detrapping.[18,19] Furthermore, a profound understanding of the

[a)]Electronic mail: biju.kp@gmail.com.
[b)]Electronic mail: ignatiev@uh.edu.
[c)]Electronic mail: hwanghs@gist.ac.kr.

resistive switching phenomena in RRAMs is required to further optimize RRAM cell operation concerning power dissipation and dispersion in switching parameters, etc. Here we studied the thickness dependent electrical switching properties of $Pt/WO_x/W$ memory devices with memory elements formed by thermal oxidation.

II. EXPERIMENTAL DETAILS

Tungsten layers of about 400 nm thickness with preferential (110) texture were prepared by sputtering at room temperature using a tungsten target on Si(001) wafers. SiO_2 films (100 nm) were deposited on top W film and were patterned using conventional photolithography. The active device size is about 250 nm. The W via defines the bottom electrode (BE) of the memory element and the size of the memory cell. These tungsten layers were then oxidized using an oxidation furnace in the temperature range of 350 °C to 500 °C for about 15–60 min in oxygen ambient. The WO_x thickness was varied from 15 to 160 nm by varying oxidation conditions.[20] Finally, a 70-nm Pt top electrode (TE) was deposited by magnetron sputtering and patterned using photolithography. To compare the pad size dependence on switching properties, cells with an active area of $50 \times 50\ \mu m^2$ were fabricated under same condition.

The structural characterization of WO_x thin films was investigated by x-ray diffraction (XRD). The cross-sectional structure of the device was investigated using Focused ion beam Scanning electron microscopy (FIB -SEM). The composition of the film was analyzed by x-ray photoelectron spectroscopy (XPS) with monochromatized Al Kα (1486.6 eV) radiation. The binding energy scale of the spectra is calibrated with respect to C 1 s signal (284.80 eV) corresponding to adventitious carbon present on the sample surface. The electrical characterization of the device was carried out using a standard parameter analyzer, Agilent 4155 C. All the bias voltage was applied to the top electrode, whereas the bottom electrode was grounded.

III. RESULTS AND DISCUSSION

XRD pattern obtained before and after thermal oxidation of W substrate was shown in Fig. 1(a). After thermal oxidation additional diffraction peaks were observed around 2θ values of 23° and 33°. Various stoichiometric and non-stoichiometric tungsten oxide compounds have rather similar crystal structures, and it is difficult to assign the XRD pattern unambiguously to a specific crystal structure. The diffraction peaks can be indexed close to the monoclinic nature of WO_3 (JCPDS 83-0950). It is observed that some of the peaks in Fig. 1(a) are broader than usual, and this could be due to the presence of a mixture of oxides. A FIB–SEM image of the typical device of thickness 30 nm was depicted in Fig. 1(b).

XPS results on thermally grown sample show the presence of tungsten, oxygen, and also some carbon due to surface contamination. Figures 2(a) and 2(b) show the W 4f spectra obtained from 15 and 49 nm tungsten oxide films before and after sputter etching. In the case of the 15 nm film, the W 4f spectra can be deconvoluted into two doublets as depicted in the Fig. 2(a). The binding energies of the first doublet are at 35.7 eV (W $4f_{7/2}$)and 37.9 eV (W $4f_{5/2}$) corresponds to the W^{6+} oxidation state. The second doublet has binding energies at 31.5 (W $4f_{7/2}$) and 33.7 eV (W $4f_{5/2}$) corresponding to the W^0 oxidation state. This indicates the incomplete oxidation for the films prepared at low annealing temperature (350 °C). After sputter etching with Ar ions (~2 nm), a significant contribution from sub oxides such as W^{5+} was also observed. However, no signal corresponding to the W^0 state was observed from the 49 nm WO_x, indicating complete oxidation of W (Fig. 2(b)). After sputter etching with Ar ions, the presence of sub oxides (W^{5+}) was still seen. The percentages of W^{6+} and W^{5+} are calculated as 93% and 7%, respectively. The presence of multiple oxidation states for W indicates that the thermally oxidize WO_x is not stoichiometric. Further the

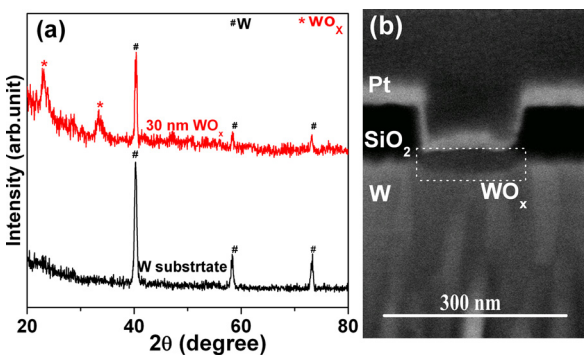

FIG. 1. (Color online) (a) XRD pattern of W substrates before and after thermal oxidation. (b) FIB- SEM image of 30 nm WO_x device formed by thermal oxidation.

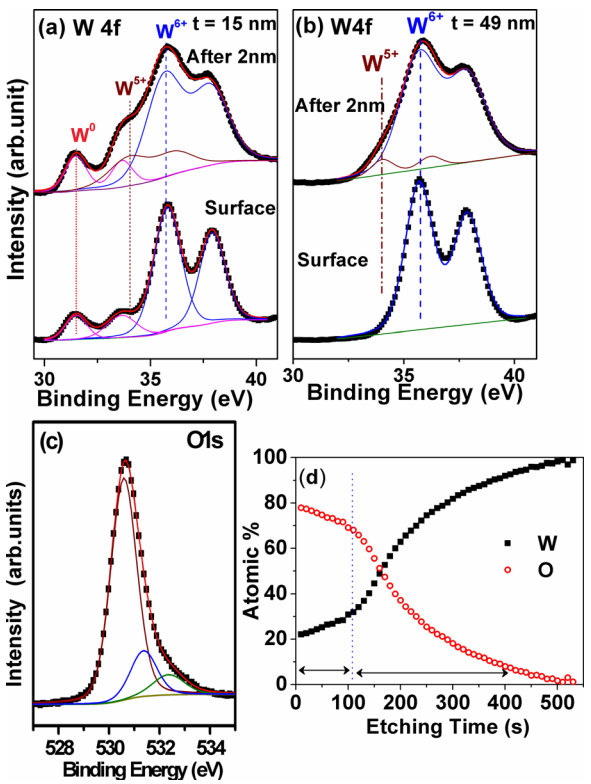

FIG. 2. (Color online) XPS spectra obtained after thermal oxidation. Core level spectra of W 4f at the surface and after sputter etching 2 nm for WO_x thickness (a) 15 nm (b) 49 nm (c) Core level spectra of O 1s (d) XPS depth profile of WO_x active layer.

O 1 s spectra have been deconvoluted into three components (Fig. 2(c)). The first component (major component) has a binding energy of 530.6 eV (76%) that is assigned to the oxygen atoms in stoichiometricWO_3. The second component observed at 531.4 eV (16%) has been attributed to O atoms in sub-stoichiometric WO_x structures. The third component is at 532.4 eV (8%), and it is assigned to the oxygen in water molecules bound to the film structure or adsorbed on the sample surface.[21] Depth wise XPS study of the WO_x suggested the presence of stoichiometric WO_3 on the top surface and metal rich sub-oxides closer to the bottom interface (Fig. 2(d)). The oxygen concentration decreases along with depth, and a broad oxide-metal interface appears near the bottom interface. It could be possible that during sputter etching with Ar ions can change the valance state of W. However, the O/W ratio decreases gradually, indicating a graded nature. The presence of sub oxides can be easily detected by a simple visual inspection of the color of the as grown WO_x (blue) thin film. The color of the film may be due to the presence of oxygen vacancies associated with tungsten ions in oxidation states lower (i.e., WO_{3-y} phases) than stoichiometric WO_3 (yellow).[22]

Figure 3 shows the current-voltage (*I-V*) characteristics of the Pt/WO_x/W memory device in different thickness of active layer (WO_x). Depending on the WO_x thickness (15–160 nm), two different types of switching, with opposite directions, were observed. In the case of 15-nm device, upon sweeping, the voltage in negative direction, an abrupt jump in current appeared around −1 V (dotted curve). This indicates that the device changes into a low resistance state (LRS). Conversely, as the voltage sweeps from zero to a positive value, an abrupt decrease in current appears at about 1 V, indicating device changed in to high resistance state (HRS). The *I-V* hysteresis loop was measured in the sequence $0 \rightarrow -V\text{max} \rightarrow 0 \rightarrow V\text{max} \rightarrow 0$ (indicated by arrows) and exhibited clockwise switching (CWS). A current compliance is usually used to protect the devices from breakdown and to control the resistance value of low resistance states (LRS) during the set processes. With a further increase in thickness (> 25 nm), the switching direction is reversed (solid curves). While sweeping the voltage in positive direction (~1.2 V), the device switched into a LRS, and the reset operation was carried out by applying a negative bias (approximately −1 V). The sweeping voltage was in the sequence $0 \rightarrow V\text{max} \rightarrow 0 \rightarrow -V\text{max} \rightarrow 0$, and exhibited counterclockwise switching (CCWS). The virgin *I-V* curves are asymmetric and nonlinear with weak rectifying behavior under negative polarity.[19] The rectification ratio was higher for the film prepared at higher annealing temperature or larger thickness. The *I-V* curves are asymmetric in LRS and HRS under the different polarities with the asymmetry being more pronounced at greater thicknesses. The transition from HRS to LRS was abrupt in the case of CWS while that was gradual for CCWS. Recently, Muenstermann *et al.* have reported "counter eight wise" (Filamentary) and "eight wise" (Homogenous) switching in Fe doped $SrTiO_3$ is analogous to CWS and CCWS observe in Pt/WO_x/W devices.[9] Both switching directions show the same polarity dependence during set or reset operation. The inset in Fig. 3 shows the resistance of the HRS and LRS obtained at 0.2 V for different WO_x layer thicknesses. It can be seen that resistance values of HRS and LRS were increasing with increasing thickness. After a critical thickness, the device changes its switching direction from clockwise to counter clock wise. The increasing resistance values by decreasing the oxygen vacancy concentration are also in good agreement with XPS data.

The CWS (dotted line in Fig. 3) was activated by a forming-type process. As shown in Fig. 4, the initial state of the device was highly conductive with a resistance of about 20 Ω. A negative sweep from 0 to −1 V did not change the device resistance state (curve 1). However, applying a positive bias about 1 V changes the device into HRS (curve 2). The device resistance was around 1 kΩ. By applying a positive voltage to the TE, oxygen atoms/ions get redistributed on the surface, and the device changes to a high resistance state (HRS). As depicted in Fig. 2(a), the films grown at low annealing conditions ($t = 15$ nm) exhibits the presence of metallic W. The initial state of the device was in the LRS, and after passing high current under appropriate polarity, these regions undergo oxidation. Thereafter the device can be switched into LRS with a negative bias on the TE (set operation) while a positive bias switches device from LRS to

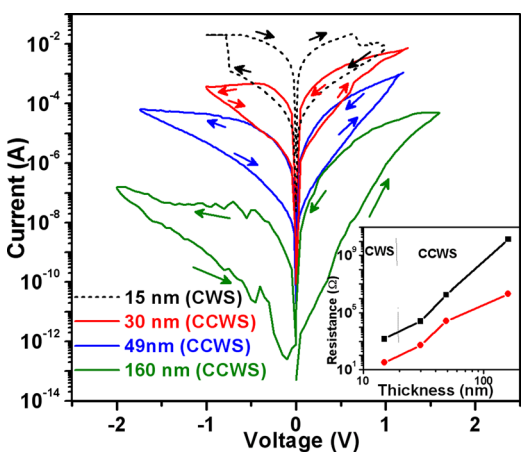

FIG. 3. (Color online) *I-V* characteristics of the Pt/WO_x/W device with different active layer (WO_x) thickness. The switching direction changes clockwise (CWS) to counter-clockwise (CCWS) with increase in thickness. Inset of Fig. 3 shows resistance of HRS and LRS as a function of WO_x thickness.

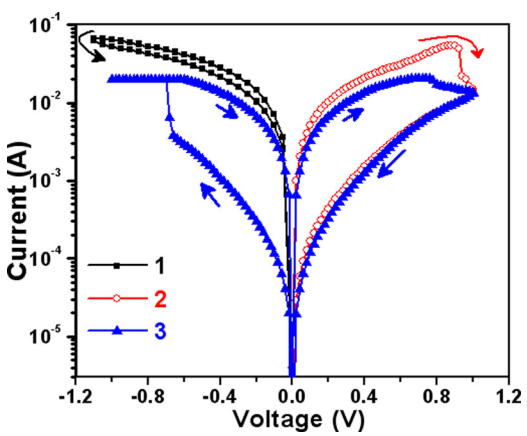

FIG. 4. (Color online) Forming type process observed in thinner film ($t \leq 15$ nm). Initial state was in the LRS (curve 1) and only positive sweep changed to HRS (curve 2).

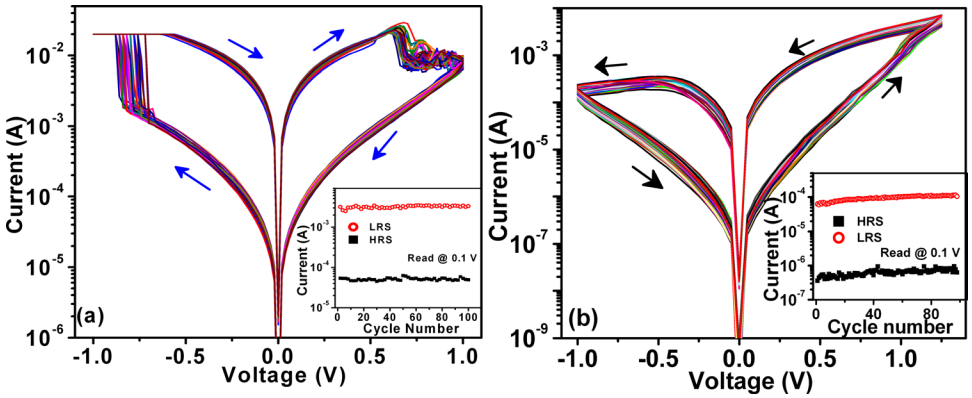

FIG. 5. (Color online) dc endurance test for the (a) CWS and (b) CCWS. Inset shows the current values of HRS and LRS measured at 0.1 V.

HRS (reset operation).[23] Hsiung *et al.* have reported forming-free TiO_2 film initially in the LRS; this is attributed to the presence of high density of oxygen-deficient defects.[24] Analogously our thinner device can be called "forming-free" device where initial state of the device is the LRS and only switched to HRS by a positive voltage. Typically, the forming voltage is much higher than the set voltage. It can degrade the device endurance and is not desirable for circuit design and testing. Therefore, it is meaningful to exploit resistive switching without the forming process. Here forming-free resistive switching in WO_x was observed by controlling the film thickness and oxidation conditions. However, with increasing thickness, the device exhibits CCWS with the initial resistance is insulating. No electroforming process is needed to be realized the RS in CCWS. The leakage current level in the HRS was found to decrease with the increase in thickness due to reduction in the oxygen vacancies. Oxygen vacancies can be regarded as n-type dopent of WO_x.

An endurance test (100 cycles) has been conducted for CWS and CCWS as depicted in Figs. 5(a) and 5(b). Both switching types exhibit good cycling endurance and are highly reproducible from device to device. The evolution of resistance of the two well-resolved states (HRS and LRS) in 100 cycles for the CWS and CCWS are depicted in the inset of Figs. 5(a) and 5(b). The resistance values were read at 0.1 V in each dc sweep. Both states are highly stable for about 100 switching cycles indicating good cycling endurance with an on/off ratio larger than 40.

To understand the pad size dependence on switching characteristics, memory cells were tested with two different active areas. As we reduced thickness to less than 30 nm, the memory cells exhibit ohmic type behavior under large area (50 μm $\times$ 50 μm) due to a large number of defects. A film thickness of about 49 nm or above shows clear CCWS. *I-V* characteristics of the WO_x device, with a thickness of 49 nm of different active areas, is depicted in Fig. 6. The resistance values of HRS and LRS follow the scaling behavior with the decrease in active area indicating no localized conduction path (inset of Fig. 6). The significant reduction in the set and reset voltage for large area device indicates that defect density is much higher. Additionally the LRS did not follow the exact scaling behavior of the HRS; this might be due to additional contributions from extrinsic defects such as grain boundaries. We suspect that there exist some percolation paths in large area devices (50 μm $\times$ 50 μm). Again the large area device shows a smaller on/off ratio ($\sim$4) with significant fluctuation in HRS. However, the small area device shows a large on/off ratio ($\sim$40) with negligible fluctuation in the LRS and HRS. This indicates the importance of device scaling on RRAM performance. Further, temperature dependent resistance of HRS and LRS has been studied for different types of switching (not shown). The LRS in the CWS shows typical metallic behavior as the resistance value was found to increase with an increase in temperature. This indicates the existence of a conduction path between the top and bottom electrodes. However, HRS and LRS in the CCWS and HRS in CWS show semiconducting behavior, indicating thermally activated transport. The possible carrier transport mechanism in LRS of the CCWS might be due to electron hoping through the defects (oxygen vacancy) giving negative temperature resistance dependence. The transport can be well fitted with equation

$$R = R_o \exp(-E_a/kT), \tag{1}$$

where R_o is a constant independent of temperature, E_a is the activation energy for charge carriers, k the Boltzmann's constant, and T the temperature. The calculated activation energies are in the range of 0.15–0.3 eV corresponding to the electronic type process.

To understand the origin of resistive switching characteristics of WO_x thin films in detail, the curve fittings of

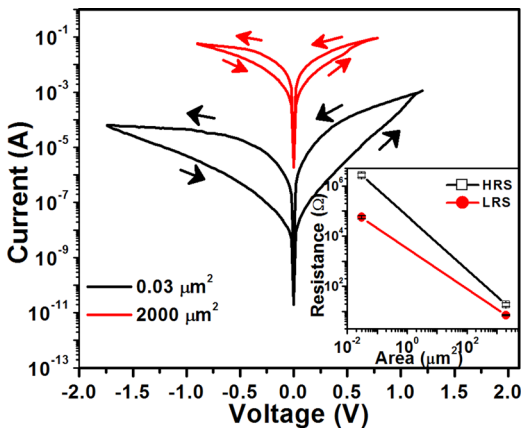

FIG. 6. (Color online) Pad size dependence of the *I-V* curve for the CCWS. Inset shows statistical distribution of the HRS and LRS with different active area.

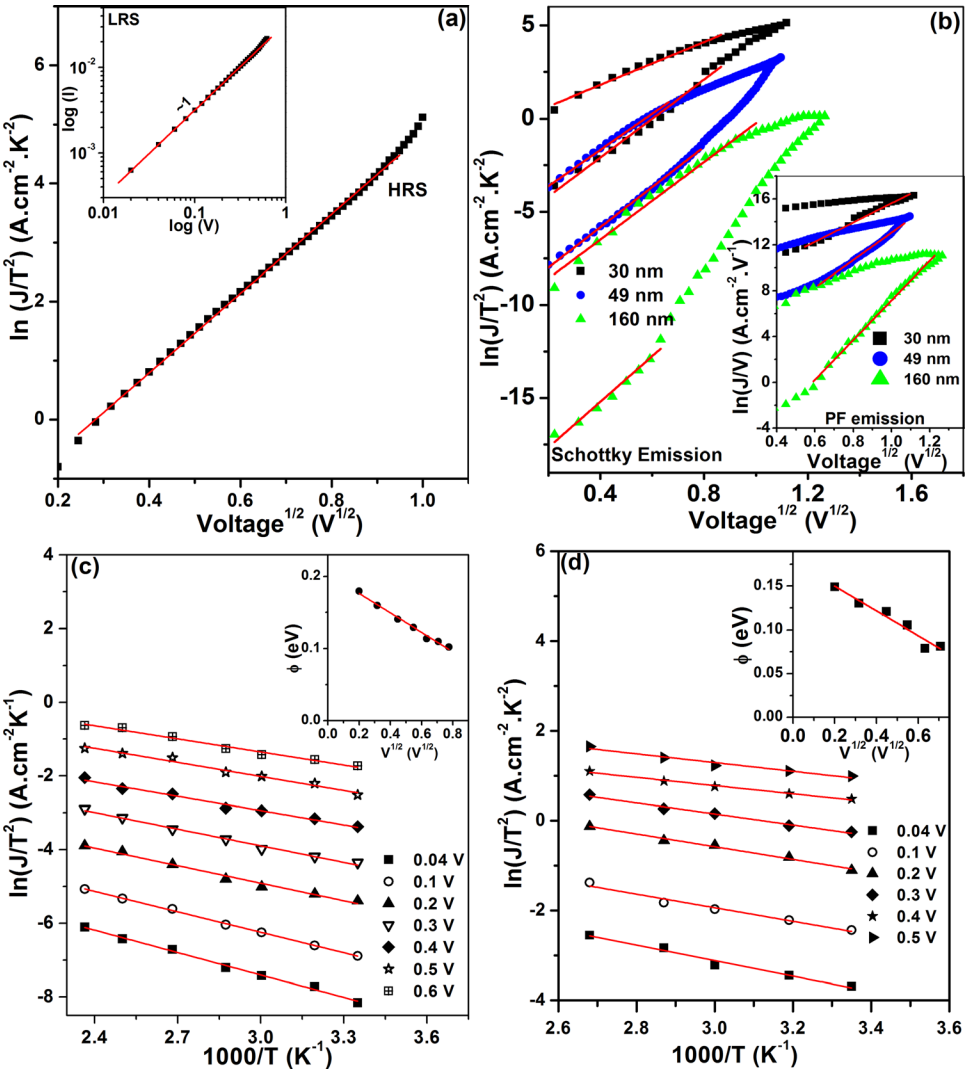

FIG. 7. (Color online) (a) *I-V* curve fitting plots for the HRS in CWS. The off state can be fitted to the Schottky emission type conduction. The inset shows LRS follows ohmic conduction behavior. (b) HRS and LRS shows Schottky emission type conduction in the CCWS. Inset shows at higher electric field HRS conduction is dominated by Poole-Frenkel emission. (c) The conventional Richardson plot (Ln (J/T^2) vs $1000/T$) for the HRS of Pt/WO_x /W stack. The inset shows the variation in Schottky barrier height as a function of the square root of the voltage. (d) The conventional Richardson plot (Ln (J/T^2) vs $1000/T$) for the LRS of Pt/WO_x /W stack. The inset shows the variation in Schottky barrier height as a function of the square root of the voltage.

conduction mechanisms for HRS and LRS in Pt/WO_x/W devices were performed. CWS shows a symmetrical LRS under different polarity which can be well fitted to ohmic type conduction (inset of Fig. 7(a)). However, the experimental *I-V* curve in the HRS shows a nonlinear relation that seems to have different conducting behaviors depending on the applied electric field. The linear relation of $\ln(J/T^2)$ versus $V^{1/2}$ indicates that the Schottky emission is the controlling conduction mechanism in HRS as depicted in Fig. 7(a). The *I-V* curves follow Schottky emission type conduction as described by

$$j = A^* T^2 \exp\left[\frac{-q(\phi - \sqrt{qV/4\pi\varepsilon d})}{kT}\right], \qquad (2)$$

where A^* is the effective Richardson constant, Φ is the barrier height, ε is the dynamic dielectric permittivity, and d is the thickness. Hence under negative bias, oxygen vacancies that accumulate at the TE lead to the collapse of the Schottky barrier.[1,2,14] The conduction in LRS can be explained by the filamentary conduction model; as the electric field is applied in the HRS, the defects such as oxygen vacancies and metal ions are likely to be populated and aligned to form the filamentary conducting paths along the grain boundaries and dislocations. This leads to the local bypass of the Schottky barrier between Pt and WO_x. However, the conduction mechanism in CCWS is different from CWS. The *I-V* curve for the HRS and LRS in the low voltage region can be well fitted to the Schottky type conduction (Fig. 7(b)), which is expected to be caused by attenuation of metal-insulator barrier due to the interaction with the electric field at the interface. To confirm the Schottky type electron injection at the Pt/WO_x interface, the *I-V* curves of HRS and LRS were measured at different temperatures for 49 nm WO_x film. Figures 7(c) and 7(d) shows the results of the *I-V* fitting to Schottky conduction so-called Richardson plot $(ln(J/T)^2$ versus $1000/T)$. The Schottky barrier height under given bias voltage was achieved and is plotted as a function square root of the voltage. By extrapolating to $V = 0$, the Schottky barrier height is determined to be 0.20 eV for HRS (inset of Fig. 7(c)) while 0.16 eV for LRS (inset of Fig. 7(d)). The HRS conduction at a higher electric field region, *I-V* curve follows Poole–Frenkel (PF) emission as shown in the right inset of Fig. 7(b). The conduction behavior of PF emission in HRS can be expressed as

$$\mathrm{In}(I/V) \propto \sqrt{e^3/(\lambda\pi\varepsilon dkT)}\sqrt{V}, \qquad (3)$$

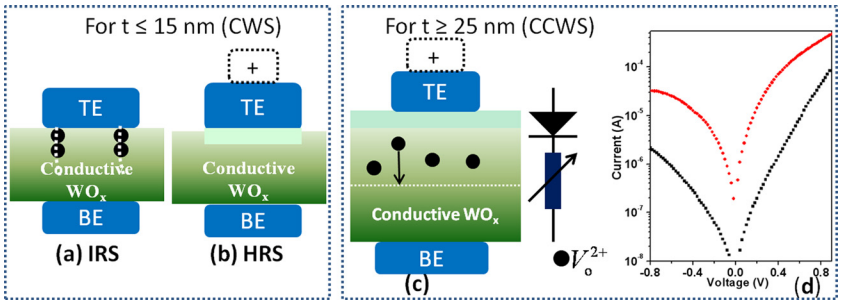

FIG. 8. (Color online) Schematic model to explain both type of switching behavior in $Pt/WO_x/W$ devices.

where λ is constant ranged between 1 and 2.[25,26] For normal PF emission, $\lambda = 1$, and when the dielectric has some trapped charges, the conduction is called the modified PF emission and in this case $\lambda = 2$. The linear relation between ln (I/V) and $\sqrt{V}$ indicates the conduction mechanism of HRS at the high electric field is dominated by Poole–Frenkel emission due to field-assisted thermal excitation of trapped electrons into the conduction band and the trapping centers provided by defects at a given moderate electric field.[25] As the conduction mechanism Pool–Frenkel is related to trap sites in the insulating material, we suggests that in HRS, most of the stoichiometric WO_3 region is composed of the high resistance phase, while a residual of the other sub oxides or oxygen vacancies act as the defect traps. The voltage range for the Poole–Frenkel emission is found increasing with the increase in thickness due to high insulating nature of the film.

A simplified model is used to explain the switching mechanism as depicted in Fig. 8. In the case of thinner films ($t \leq 15$ nm), initial state of the device was leaky due to insufficient oxidation or the existence of some percolation path in the film (Fig. 8(a)). When we apply positive bias to the Pt TE, oxygen ions/atoms move to the top interface and oxidize the conducting path. Now the device changes to the high resistance state (Fig. 8(b)). It may be possible that the oxidation might be assisted by Joule heating. It is noted that the high work function Pt (5.65 eV) TE and n-type WO_x interface forms a Schottky barrier, whereas the bottom electrode (BE) interface of WO_x/W is considered a quasi-ohmic contact because of the generation of a high concentration of oxygen vacancies during oxidation process. By applying negative voltage, the oxygen vacancies are accumulated at the Pt top electrode through the grain boundaries. This caused the collapse of the Schottky barrier, resulting transition from HRS to LRS, making a filamentary conducting path. The conducting filament locally bypasses the Schottky-like interface barrier between oxide material and top electrode. On the other hand, by applying positive voltage, the oxygen was brought to the top electrode Pt and WO_x interface as well as rupture of conducting channels by oxidation transforming to HRS. The film with thickness greater than 25 nm shows asymmetric *I-V* curves indicating an existence of Schottky type barrier at the top interface. Hence we believe the switching location may be at the bottom interface (Fig. 8(d)). Upon applying positive bias at the top electrode, oxygen vacancies piled up at the bottom interface (Fig. 8(c)). This leads to the reduction of the WO_x layer at the bottom interface and switches the device into LRS. Conversely applying a negative bias to the TE, the reduced WO_x is oxidized again and hence the device switches into HRS. The asymmetry in the *I-V* curve was originated from the top interface. As the annealing temperature increases, there is significant reduction in the oxygen vacancy concentration in the active layer. It has also been observed from XPS that there is a significant reduction in the sub oxides close to the top interface with higher annealing temperature. This leads to more asymmetrical *I-V* curve due to the increase in effective Schottky barrier height. Additionally it may be possible that new oxygen vacancies are created due to excorporation of oxygen through Pt TE under positive bias. It is interesting to see that when switching at the bottom interface, more uniform movement of oxygen vacancies leads to homogeneous type resistive switching. This may be due to non homogenous distribution of defects such as oxygen vacancies across the active layer. The observed behavior is due to inherent nature of thermal oxidation. Further investigation is needed for the barrier modulation at the Pt/WO_x interface by electron trapping and detraping.[10,20]

A retention test has been conducted on both types of switching as depicted in Fig. 9. As shown in Fig. 9, a voltage signal of 0.1 V was adopted to read the current of HRS and LRS. Moderate retention was observed for CCWS, while it was good for CWS. The LRS in the CCWS exhibits a gradual decrease in the resistance or current with time. The gradual decrease in the resistance level might be due to diffusion of the ionic species or detrapping of electrons. The expected retention was calculated by extrapolating the LRS and found

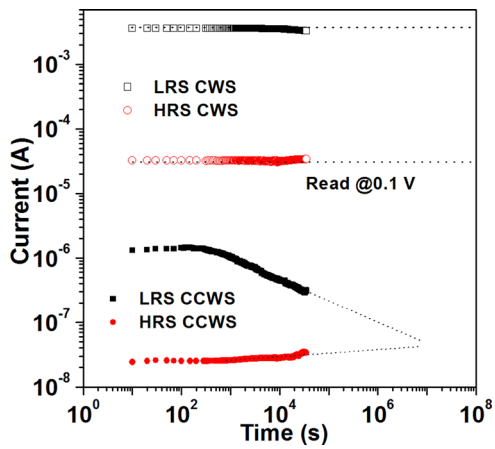

FIG. 9. (Color online) Retention characteristics of $Pt/WO_x/W$ memory device measured at room temperature for CWS and CCWS under a reading voltage of 0.1 V.

to be a month. Generally, the retention characteristics of interface-type resistive switching device were not very good. However, LRS in CWS was highly stable with no obvious degradation even after 10 hr. This also indicates two different types of switching shows different memory characteristics and both coexist in the same material.

IV. CONCLUSIONS

We studied resistive the switching characteristics of $Pt/WO_x/W$ memory devices. By varying active layer thickness, two resistance switching modes were observed in WO_x film. Thinner films ($t < 15$ nm) exhibit a clockwise switching with filamentary characteristics. With the increase in thickness, the switching direction changed into counter-clockwise with more homogeneous type conduction. In the case CWS, the conduction changes from Schottky emission to ohmic conduction due to the local bypass of the Schottky barrier between Pt and WO_x. For CCWS, the conduction mechanism in HRS is Schottky emission at low electric field and Poole–Frenkel emission which is at high electric field, is changed to the Schottky emission in LRS. The observed behavior may be attributed to the inhomogeneous defect distribution across the sample due to the inherent nature of the thermal oxidation. A moderate retention was observed for CCWS, whereas an excellent retention was observed in CWS.

ACKNOWLEDGMENTS

This work was supported by the National Research Laboratory (NRL) Program and the World Class University (WCU) program of the National Research Foundation (NRF).

[1]R. Waser, R. Dittmann, G. Staikov, and K. Szot, Adv. Mater. **21**, 2632 (2009).
[2]J. J. Yang, M. Pickett, X. Li, D. Ohlberg, D. Stewart, and R. S. Williams, Nat. Nanotechnol. **3**, 429 (2008).
[3]I.-G. Baek, D. C. Kim, M. J. Lee, H.-J. Kim, M. S. Lee, J. E. Lee, S. E. Ahn, S. Seo, J. H. Lee, J. C. Park, Y. K. Cha, S. O. Park, H. S. Kim, I. K. Yoo, U- In Chung, J. T. Moon, and B. I. Ryu, Tech. Dig. Int. Electron Devices Meet. **2005**, 750 (2005).
[4]A. Sawa, Mater. Today **11**, 28 (2008).
[5]L. Goux, J. G. Lisoni, M. Jurczak, D. J. Wouters, L. Courtade, and Ch. Muller, J. Appl. Phys. **107**, 024512 (2010).
[6]D. S. Jeong, H. Schroeder, and R. Waser, Electrochem.Solid-State Lett. **10**, G51 (2007).
[7]W. Shen, R. Dittmann, and R. Waser, J. Appl. Phys. **107**, 094506 (2010).
[8]S. Lee, H. Kim, J. Park, and K. Yong, J. Appl. Phys. **108**, 076101 (2010).
[9]R. Muenstermann, T. Menke, R. Dittmann, and R. Waser, Adv. Mater. **22**, 4819 (2010).
[10]K. Shibuya, R. Dittmann, S. Mi, and R. Waser, Adv. Mater. **22**, 411 (2010).
[11]K. M. Kim, B. J. Choi, Y. C. Shin, S. Choi, and C. S. Hwang, Appl. Phys. Lett. **91**, 012907 (2007).
[12]K. M. Kim, B. J. Choi, S. J. Song, G. H. Kim, and C. S. Hwang, J. Electrochem. Soc. **156**, G213 (2009).
[13]U. Russo, D. Jelmini, C. Cagli, A. L. Lacaita, S. Spiga, C. Wiemer, M. Perego, and M. Fanciulli, Tech. Dig. Int. Electron Devices Meet. **2007**, 775 (2007).
[14]H. Shima, N. Zhong, and H. Akinaga, Appl. Phys. Lett. **94**, 082905 (2009).
[15]H. Y. Peng, G. P. Li, J. Y. Ye, Z. P. Wei, Z. Zhang, D. D. Wang, G. Z. Xing, and T. Wu, Appl. Phys. Lett. **96**, 192113 (2010).
[16]M. N. Kozicki, C. Gopalan, M. Balakrishnan, and M. Mitkova, IEEE Trans. Nanotechnol. **5**, 535 (2006).
[17]C. H. Ho, E. K. Lai, M. D. Lee, C. L. Pan, Y. D. Yao, K. Y. Hsieh, R. Liu, and C. Y. Lu, Dig. Tech. Pap.-Symp. VLSI Technol. **2007**, 228 (2007).
[18]W. C. Chien, Y. C. Chen, E. K. Lai, Y. D. Yao, P. Lin, S. F. Horng, J. Gong, T. H. Chou, H. M. Lin, M. N. Chang, Y. H. Shih, K. Y. Hsieh, R. Liu, and C.-Y. Lu, IEEE Electron Device Lett. **31**, 126 (2010).
[19]D. S. Shang, L. Shi, J. R. Sun, B. G. Shen, F. Zhuge, R. W. Li, and Y. G. Zhao, Appl. Phys. Lett. **96** 72103 (2010).
[20]R. Sohal, C. Walczyk, P. Zaumseil, D. Wolansky, A. Fox, B. Tillack, H.-J. Mussig, and T. Schroeder, Thin Solid Films **517**, 4534 (2009).
[21]Ch. D. Wagner, A. V. Naumkin, A. Kraut-Vass, J. W. Allison, C. J. Powell, and J. R. Rumble, Jr., See http://srdata.nist.gov/xps/ for information on NIST Standard Reference Database 20, Version 3.4 (2003).
[22]A. Rougier, F. Portemer, A. Quede, and M. El Marssi, App. Surf. Sci. **153**, 1 (1999).
[23]E. K. Lai, W. C. Chien, Y. C. Chen, T. J. Hong, Y. Y. Lin, K. P. Chang, Y. D. Yao, P. Lin, S. F. Horng, J. Gong, S.C. Tsai, C. H. Lee, S. H. Hsieh, C. F. Chen, Y. H. Shih, K. Y. Hsieh, R. Liu, and C. Y. Lu, Jpn. J. Appl. Phys. **49**, 04DD17 (2010).
[24]C.-P. Hsiung, J.-Y. Gan, S. H. Tseng, N. H. Tai, P. J. Tzeng, C.-H. Lin, F. Chen, and M.-J. Tsai, Electroochem. Solid State Lett. **12**, G31 (2009).
[25]J. G. Simmons, Phys. Rev. **155**, 657 (1967).
[26]J. R. Yeargan and H. L. Taylor, J. Appl. Phys. **39**, 5600 (1968).